

## Supporting Information for

### Virus-templated Au and Au/Pt Core/shell Nanowires and Their Electrocatalytic Activities for Fuel Cell Applications

YOUJIN LEE<sup>1\*</sup>, JUNHYUNG KIM<sup>2\*</sup>, DONG SOO YUN<sup>1</sup>, YOON SUNG NAM<sup>3</sup>,  
YANG SHAO-HORN<sup>1,2†</sup>, AND ANGELA M. BELCHER<sup>1,3†</sup>

†e-mail: [shaohorn@mit.edu](mailto:shaohorn@mit.edu), [belcher@mit.edu](mailto:belcher@mit.edu)

\* These authors contributed to this work equally.

**S1. Preparation of phage solutions**

**S2. Synthesis of Au NWs from various M13 genetic templates**

**S3. Conversion efficiency of Au NWs from different genes**

**S4. Preparation of Au NWs with different diameter sizes**

**S5. Rotating Disk Electrode Measurements for CO oxidation**

**S6. The structural confirmation of Au/Pt core/shell NWs**

**S7. Synthesis of Au/Pt core/shell NWs with various Pt loadings**

**S8. X-ray diffraction of Au/Pt core/shell NWs**

**S9. Comparison of the mapping result of Au/Pt core/shell NWs with atomic ratio of  
1:1 and 2.6:1**

**S1. Preparation of phage solutions**

The wild type M13 phage and its plasmid, M13KE, were purchased from New England Biolabs (NEB). The plasmid for p8 protein modification, M13SK, was constructed through site-directed mutagenesis: T at position 1372 and C at position 1381 were mutated to A and G respectively. This mutation creates digestion sites for Pst I and BamH I enzymes for modification of the p8 protein. The M13SK phage vector was used to construct a p8 library. The p8#9 sequence was selected from the p8 library via standard combinatorial screening against Au. In subsequent experiments, p8#9 phages were genetically constructed from the M13SK phage vector. The M13SK vector was digested with Pst I and BamH I enzymes (NEB) purified, dephosphorylated and ligated with a DNA duplex encoding the #9 peptide sequence. The oligonucleotide sequences used for Au binding are 5' GTG TCG GGG TCG TCG CCG GAT TCG 3' and 5' GAT CCG AAT CCG GCG ACG ACC CCG ACA CTG CA 3'. The ligated vector was electrotransformed into XL-1 blue *E. coli* cells and incubated briefly then plated and incubated overnight at 37 °C. The DNA of the cloned phages was sequenced to make sure the appropriate sequence was inserted. The E4 sequence was prepared in a similar manner to #9.

## **S2. Synthesis of Au NWs from various M13 genetic templates**

### **Synthesis of Au NWs from p8#9 phage:**

Au NWs with average diameter size about 40 nm were prepared by incubating 1 mL of 10 mM Au<sup>3+</sup> aqueous solution from hydrated hydrogen tetrachloroaurate (HAuCl<sub>4</sub>•3H<sub>2</sub>O, Aldrich) with p8#9 (10 mL with 3.5 x 10<sup>10</sup> pfu/mL stored in 1X TBS buffer solution, pfu: plaque forming unit) dispersed in 25 mL of 0.06 M Cetyl trimethylammonium bromide (CTAB, Aldrich) solution. Right after mixing, the solution was deep yellow, and the color got paler as Au<sup>3+</sup> ions partially reduced to Au<sup>+</sup> in the presence of amine groups both in the TBS buffer and in the phage surface. The colorless solution incubated for three hours at room temperature was further reduced by the addition of 0.15 mL of 0.1 M ascorbic acid (L-(+) ascorbic acid powder, J. Baker) and 0.15 mL of 10 mM silver nitrate (AgNO<sub>3</sub>, Alfa Aesar) solution. The diameters of Au NWs were tunable by changing the concentration of phage, CTAB, and ascorbic acid, and detailed information of each material is summarized in Table S1. Reduction of Au ions from other reducing agents such as sodium borohydride and sodium citrate did not provide continuous NW structures.

### **Synthesis from other genetic templates:**

To confirm the advantage from the specific affinity of p8#9 for the preparation of well-defined Au NWs, two genetic templates, M13KE (the wild type M13 phage) and E4 (M13 phage with four glutamates on p8 major protein), were tested. The 1X TBS buffer solution used for the storage and dispersion of p8#9 templates was also tested for the synthesis of Au NWs. From the M13 templates without specific Au-binding peptides, fine Au NPs (2 to 20 nm in diameter sizes) randomly distributed over the TEM grids

were observed. From the TBS buffer, Au NPs about 50 to 100 nm in diameter sizes were obtained.

**Removal of CTAB from NWs:** The as-synthesized Au-NWs were dispersed in 1X TBS-buffered solution with excess CTAB stably. For the analysis (both for the Inductively Coupled Plasma Optical Emission Spectroscopy (ICP-OES) and electrochemical analysis), excess CTAB and ions from buffered solution were discarded after the centrifugation (7000 rpm for 10 minutes). NWs were further washed with 95% ethanol and water mixture (1:1 volume ratio) and the NW pellet after the centrifugation was re-dispersed in either de-ionized water (for ICP-OES) or 0.05 mM CTAB solution (for electrochemical analysis). The TGA (Thermogravimetric analysis) result showed the cleaned NWs contained 2 wt% CTAB (reference 20), and the XPS data on NWs also confirmed the existence of carbon atoms (from CTAB).

### **S3. Conversion efficiency of Au NWs from different genes**

UV-Vis spectroscopy and ICP-OES were used to quantify the amount of Au<sup>3+</sup> ions converted into Au NWs for the synthesis using p8#9 phage and Au NPs in cases of using other templates such as E4 phage, wild type M13 phage, and TBS buffer. To determine the Au conversion efficiency, the final solutions of Au NWs (from p8#9) and NPs (other genes and TBS) from each experimental set were separated after centrifugation and the supernatant was transferred to another clean tube. Un-reacted Au ions remaining in the supernatant were reduced to Au random particles by adding 1M sodium borohydride (NaBH<sub>4</sub>) solution. A pink to violet color, which indicated the presence of Au, appeared within a minute in all solutions except the supernatant solution

associated with the p8#9 phage. The p8#9 supernatant showed no significant absorption over the entire UV-Vis spectrum indicating the incorporation of all of the gold into the NWs. After dissolving the precipitates collected from each experimental set in aqua regia (a mixture of hydrochloric acid and nitric acid), the amount of Au products was quantified using ICP-OES. The sum of Au ions from the Au NWs/NPs precipitates and the supernatant solution was greater than 98% in all case. The yields were 44 % for E4, 31% for wild type M13 phage, and 27% for TBS buffer.

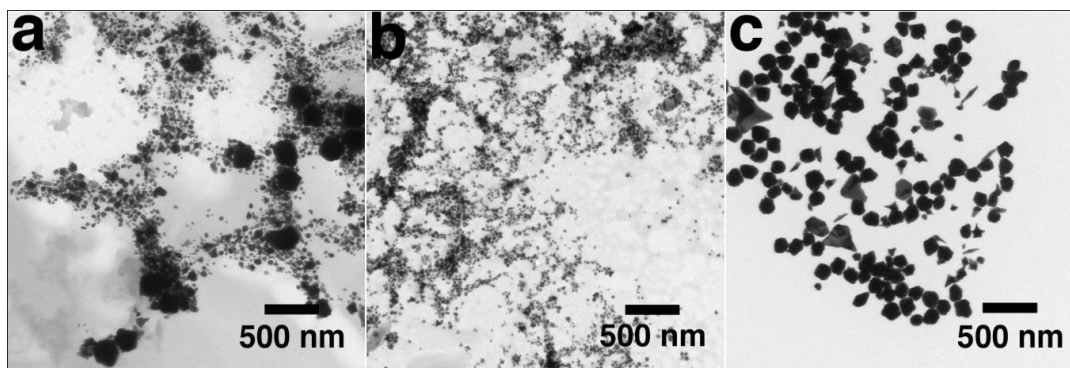
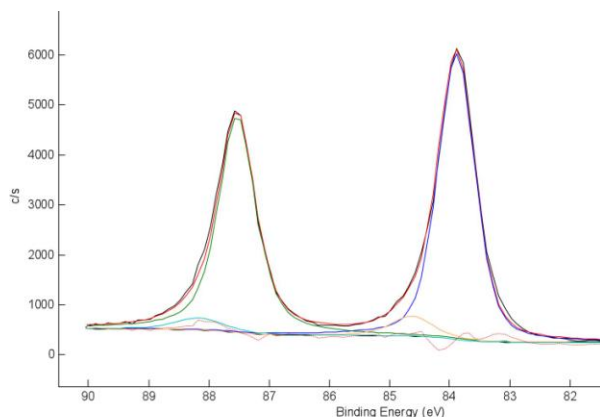


**Fig. S1. TEM images of Au NPs prepared from different genetic templates and the TBS buffers.** (a) E4 phage template, (b) wild type M13 phage, and (c) 1X TBS buffer.

Template	Product	Concentration [ppm]		Conversion efficiency [%]
		Au <sup>3+</sup>	Au product	
P8#9	15 nm x 5 um	55	53.9	98
	30 nm x 5 um	55	54.3	99
	40 nm x 5 um	55	54.1	98
E4	NPs	55	24	44
Wild type	NPs	55	17	31
TBS buffer	NPs	55	15	27

**Table S1. Conversion efficiency of Au<sup>3+</sup> ions to Au nano-structures.** P8#9 template converts more than 98 % of Au ions to Au both in Au nanowires. The top three results come from the surfactant mediated diameter controlled nanowires, and the conversion efficiencies from M13 phage with different genes yield values that are lower than 50 %.

The XPS result of Au NWs confirmed that majority (more than 97%) of Au in the NW structure is metallic Au. The ionic Au species detected in XPS could be explained either the oxidation of Au NW surfaces in the air or the intrinsic ionic clusters on top of the NWs as previously reported active catalytic component of gaseous CO oxidation.



	Binding Energy (eV)	Integrated Area (%)
Au 4f <sub>7/2</sub>	83.9	52.94
Au 4f <sub>5/2</sub>	87.6	44.14

**Fig. S2. XPS result of Au NWs and Table S1. Metallic Au species in Au NWs.**

#### **S4. Preparation of Au NWs with different diameter sizes**

The diameters of Au NWs were tunable by changing the concentration of phage, CTAB, and ascorbic acid, and detailed information of each material is summarized in Table S1 and TEM images are available in Fig. S2. All units in Table S1 are molar concentration [mol/L] and the total volume of the reaction solution ranged from 30 mL to 38 mL. The diameter of Au NWs was thickened from 10 nm to 30 nm by changing the concentration of CTAB and ascorbic acid, but there was a limitation when increasing the diameter to over 30 nm. The Au NWs with 38 and 50 nm diameters were formed when we doubled the concentration of phage solution by adjusting the amount of other reactants properly. Because we used p8#9 stored in 1X TBS buffer solution, 5 mL of TBS was added to the synthesis of 30 nm Au NWs to dilute the phage concentration.

The reproducibility of Au NWs here is affected by the concentration of p8#9, which is usually determined by counting the active colonies from the power dilution of original phage solution after each amplification, so there possibly be shift in mean-diameter-sizes in the synthesis from different p8#9 phage solution, but the homogeneity and the distribution of diameter size are maintained. The NWs reported here are all prepared from one phage amplification batch, therefore there is no deviation between phage stock here. The TEM images shown in Fig. S2 were prepared from six different reactions to control the diameter sizes, and the average diameter obtained from the statistical calculation deviated slightly from the protocol. The average diameters of each sample in Fig. S2 are 9, 18, 24, 31, 38, and 50 nm from the protocol for the preparation methods of 10, 20, 25, 30, 40, and 50 nm, respectively.

## Size distribution of Au NWs

The diameter sizes of synthesized Au NWs from the change in reactant solution shown in Table S1 usually results shift less than 3 nm in average diameter size with similar size distribution due to the errors in phage concentration from the colony counting after each amplification step. Figure S3 is the histogram of six different synthetic conditions shown in Fig. 3 in the manuscript. The average diameter of each sample was determined statistical methods after measuring the diameter of Au NWs more than 500 positions, where the zone axis can be defined.

Average diameter	CTAB [M]	P8#9 [pfu/mL]	Au <sup>3+</sup> [M]	Ascorbic acid [M]	Ag <sup>+</sup> [M]
50 nm	0.041	9.45 X 10 <sup>9</sup>	4.1 X 10 <sup>-4</sup>	8.1 X 10 <sup>-4</sup>	6.1 X 10 <sup>-5</sup>
40 nm	0.041	9.60 X 10 <sup>9</sup>	2.7 X 10 <sup>-4</sup>	8.2 X 10 <sup>-4</sup>	4.1 X 10 <sup>-5</sup>
30 nm	0.041	4.80 X 10 <sup>9</sup>	2.7 X 10 <sup>-4</sup>	8.2 X 10 <sup>-4</sup>	4.1 X 10 <sup>-5</sup>
25 nm	0.048	5.59 X 10 <sup>9</sup>	3.2 X 10 <sup>-4</sup>	4.8 X 10 <sup>-4</sup>	4.8 X 10 <sup>-5</sup>
20 nm	0.080	5.59 X 10 <sup>9</sup>	3.2 X 10 <sup>-4</sup>	4.8 X 10 <sup>-4</sup>	4.8 X 10 <sup>-5</sup>
10 nm	0.082	5.71 X 10 <sup>9</sup>	1.6 X 10 <sup>-4</sup>	2.4 X 10 <sup>-4</sup>	2.4 X 10 <sup>-5</sup>

**Table S3. Table of concentrations for the preparation of Au NWs with different diameters.**

All the concentration except phage is in M [mol/Liter]. The unit for the phage concentration, pfu, means plaque-forming unit of M13 phages. The total volume of each synthesis varied from 30 mL to 38 mL.

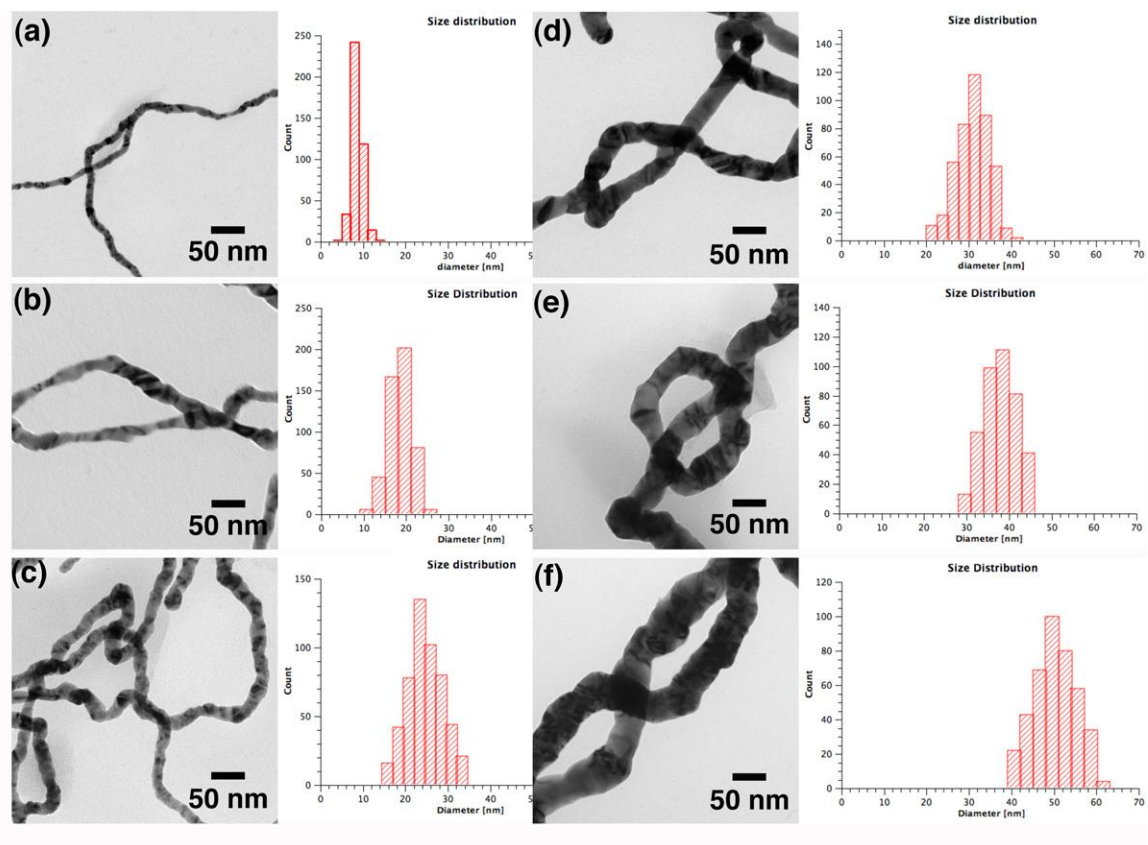


**Fig. S3. Au NWs with different diameters.** Au NWs with various diameter sizes were prepared by changing the concentration of phage, CTAB, and precursors. The TEM images were taken at a same magnification at 41K to compare the sizes. Due to the surface roughness between smaller crystalline domains in the NWs, the NWs show deviations. The average diameter value with the standard deviation are (a)  $9\pm 1.3$  nm, (b)  $18\pm 2.7$  nm, (c)  $24\pm 4.1$  nm, (d)  $31\pm 3.8$  nm, (e)  $38\pm 4.0$  nm, and (f)  $50\pm 4.8$  nm.

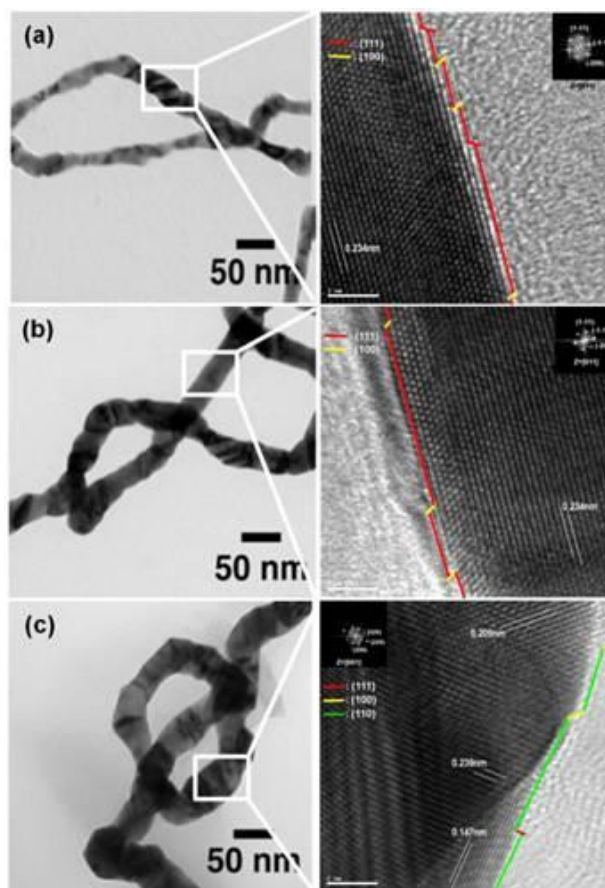


**Fig. S4. TEM images of (a)  $20 \pm 0.3$  nm, (b)  $30 \pm 0.3$  nm and (c)  $40 \pm 0.3$  nm Au NWs and HRTEM.** The crystallographic analysis on the surface of Au NWs revealed that the 20 nm and 30 nm of Au NWs grew along the (111) direction (show a NW with lattice fringe of 0.23 nm corresponding to the (111) lattice spacing). On the other hand, 40 nm diameter of the Au NWs showed different surface crystal structure (110).

## **S5. Rotating Disk Electrode Measurements for CO oxidation**

### **Preparation of working electrodes**

A 20  $\mu\text{L}$  solution of the Au NWs suspension in Milli-Q water was applied onto a glassy carbon disk electrode ( $0.196\text{ cm}^2$  geometrical surface area) substrate at a Au NW loading of a several  $\mu\text{g}$ . After evaporating the solvent, the deposited Au NWs thin film was covered with 15  $\mu\text{L}$  of 0.05 wt% Nafion<sup>®</sup> solution to attach the Au NWs to the glassy carbon disk. The electrode was then dried under air atmosphere with a cover glass and transferred to the electrochemical cell in Ar saturated 0.1 M KOH electrolyte.

### **Electrochemical measurements**

The electrochemical studies were carried out in a three-electrode cell using a saturated calomel electrode (SCE) as the reference and a platinum wire as the counter electrode. The electrochemical measurements were conducted by using a voltamaster potentiostat (Radiometer analytical, France). All potentials, however, are referenced to the reversible hydrogen electrode (RHE) potential, calibrated via the hydrogen oxidation/reduction reaction on a pure Pt rotating disk electrode in the same cell and electrolyte at the same temperature. Cyclic voltammetry (CV) was conducted at a scan rate of 20 mV/s in Argon-saturated 0.1 M KOH electrolyte and the continuous oxidation of CO was measured in CO-saturated 0.1 M KOH after bubbling CO for 25 min. In the rotating disk electrode (RDE) experiments, the working electrode was rotated in the range of 100 - 2500 rpm using a PINE Instruments AFMSRCE rotator. The electrode potential was maintained at -0.20 V (RHE) for 1 min prior to recording the positive potential sweep.

### Determination of electrochemical surface area (ESA) of Au NWs

A cyclic voltammogram (CV) of Au NWs/GCE in Fig S4 shows that increasing potential in the Ar-saturated 0.1 M KOH solution in the positive sweep led to increasing current, which is associated with adsorption of oxygenated species and the formation of oxides on the Au surface at potentials greater than  $\sim 1.2$  V vs. RHE. In the negative sweep, surface oxides were reduced as indicated by a single reduction peak in the cathodic potential scan at  $\sim 1.05$  V vs. RHE. The charge associated with oxide reduction on Au was obtained from integrating current in the CV data (color region in Fig S4) after double layer current subtraction. Based on  $240 \mu\text{C}/\text{cm}^2_{\text{Au}}$  for surface oxide reduction reported previously,<sup>1</sup> the electrochemical surface area (ESA) of Au NWs was calculated.

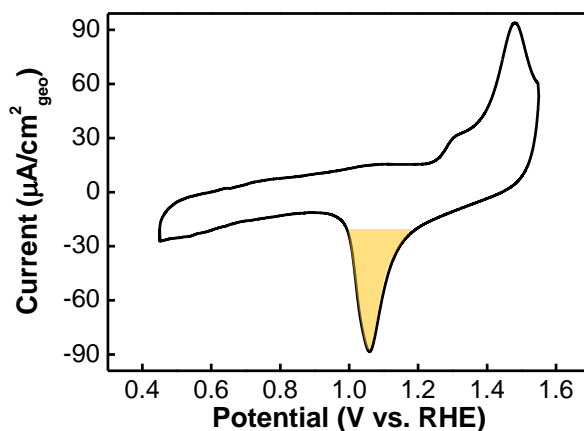


**Fig. S5.** Cyclic voltammogram of 20 nm Au NWs supported on GCE (loading of  $16.3 \mu\text{g}/\text{cm}^2$ ) in Ar-saturated 0.1 M KOH at a scan rate of 20 mV/s.

### Analysis of kinetic current from RDE measurements

Geometric RDE current density ( $\text{mA}/\text{cm}^2_{\text{geo}}$ ) consists of kinetic and diffusion components,  $i_k$  and  $i_d$ , respectively, which is accomplished with the following relation, so called Koutecky-Levich equation (1, #60)

$$\frac{1}{i} = \frac{1}{i_k} + \frac{1}{i_d} = \frac{1}{nFAkc_0} + \frac{1}{0.62nFAD_{\text{CO}}^{2/3}\nu^{-1/6}c_0\omega^{1/2}} \quad (1, \#60)$$

where  $i$  is the measured current,  $n$  is the number of electrons in the CO oxidation reaction,  $F$  is the Faraday constant,  $A$  is the geometric electrode area,  $D$  is the diffusion coefficient of CO in solution,  $\nu$  is the kinematic viscosity of the electrolyte,  $c_0$  is the CO solubility in the electrolyte, and  $\omega$  is the rotation rate. Equation (1, #60) can be simply formed by equation (2).

$$\frac{1}{i} = \frac{1}{i_k} + \frac{1}{Bc_0\omega^{1/2}} \quad (2)$$

The Koutecky-Levich plots ( $i^{-1}$  vs  $\omega^{-1/2}$ ) at four different potentials 1.02, 1.20 V vs. RHE in the positive sweep and 0.80 and 0.60 V vs. RHE in the negative sweep are shown in Fig. S5(a) – (c), where kinetic currents for CO oxidation,  $i_k$ , were calculated based on the equation (1, #60); having these  $Bc_0$  values (Fig. S5, Equation 2), kinetic currents ( $i_k$ , #37) as a function of potential were calculated from equation 3.

$$i_k = \frac{i \times i_d}{i_d - i} \quad (3)$$

All the slopes were found similar at different potentials with an average Levich slope of  $Bc_0 = 5.35 \times 10^{-2} \text{ mA}/\text{cm}^2/\text{rpm}^{1/2}$ ,  $5.54 \times 10^{-2} \text{ mA}/\text{cm}^2/\text{rpm}^{1/2}$ ,  $5.00 \times 10^{-2} \text{ mA}/\text{cm}^2/\text{rpm}^{1/2}$  for Au NWs of 20 nm, 30 nm and 40 nm, respectively. The experimental values of the

Levich slope are in agreement with the calculated value of  $Bc_0 = 5.54 \times 10^{-2}$  mA/cm<sup>2</sup>/rpm<sup>1/2</sup> from equation 2, based on the solubility of CO ( $c_0 = 0.96 \times 10^{-7}$  mol/cm<sup>3</sup>), the kinematic viscosity of the electrolyte ( $\nu = 1.07 \times 10^{-2}$  cm<sup>2</sup>/s) and its diffusivity ( $D = 1.8 \times 10^{-5}$  cm<sup>2</sup>/s) for a two-electron oxidation process.

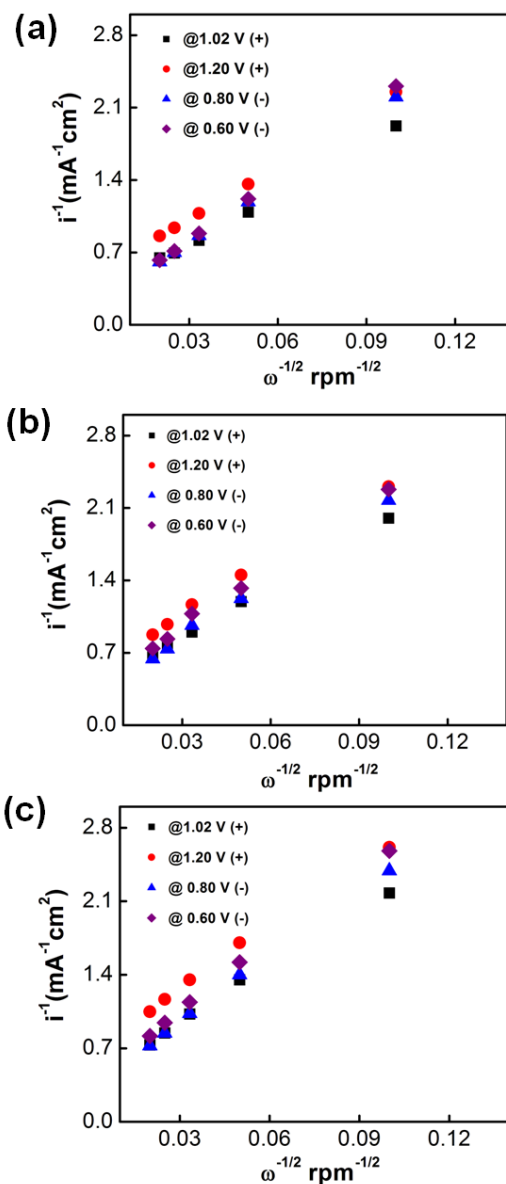


**Fig. S6.** Koutecky-Levich analysis of the CO oxidation data on the different diameters of Au NWs/GCE in Figure 3(c) ~ (e) at 1.02 V(+), 1.20 V(+), 0.8 V(-), and 0.6 V (-), (+): positive-going sweep and (-): negative-going sweep.

### S6. The structural confirmation of Au/Pt core/shell NWs

The dark field TEM analysis of Au/Pt core/shell NWs with atomic ratio of 1:1 confirmed the existence of Au as core and Pt as outer shell as shown in Fig. S6. The Au atoms are more concentrated on the center (Fig. S6B) and the Pt atoms are broadly distributed (Fig. S6C). The TEM images of Au/Pt core/shell NWs with various Pt loading clearly show the different thickness of NWs as shown in Fig S6.

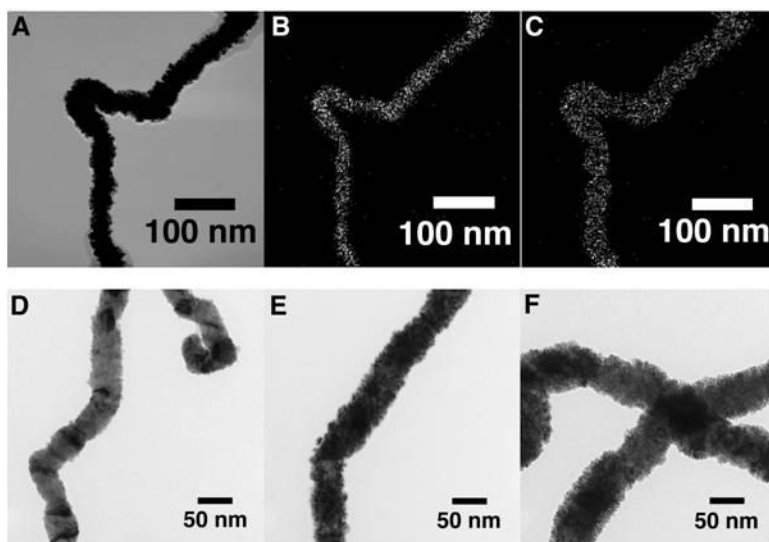


**Fig. S7. TEM analysis of Au/Pt core/shell NWs.** Dark field TEM analysis clearly visualizes the distribution of Au(B) and Pt(C) atoms in core/shell NWs. As the concentration of Pt precursor increased, the coverage of Pt NPs also increased and Au/Pt core/shell NWs with various Au:Pt atomic ratios (D-2.6:1, E-1.8:1, and F-1:1) were prepared.

### S7. Synthesis of Au/Pt core/shell NWs with various Pt loadings

For the preparation of Au/Pt core/shell NWs with 1:1 atomic ratio of Au:Pt, 3 mL of homogeneous as-synthesized Au NW solution was transferred to a 15 mL falcone tube, and 200  $\mu\text{L}$  of 10 mM  $\text{Pt}^{4+}$  solution from chloroplatinic acid hexahydrate ( $\text{H}_2\text{PtCl}_6 \cdot 6\text{H}_2\text{O}$ ) was added. The solution was incubated for two hours in a rocking machine with gentle shaking to induce  $\text{Pt}^{4+}$  ions to the surface of Au NWs, and then 400  $\mu\text{L}$  of 0.1 M ascorbic acid was added to reduce  $\text{Pt}^{4+}$  ions to Pt nano-shells. The solution was kept at 50  $^\circ\text{C}$  for overnight without agitation. The information of the concentration of Pt and ascorbic acid for the preparation of Au/Pt core/shell NWs with various Au:Pt atomic ratios is available in Table S2.

Au:Pt atomic ratio	Au NWs [mM]	$\text{Pt}^{4+}$ [mM]	Ascorbic acid [mM]
1:0	0.274	0	0
2.6:1.0	0.249	0.30	6.06
1.8:1.0	0.238	0.43	8.70
1.0:1.0	0.228	0.56	11.1

**Table S4. Summary of concentration for the preparation of Au/Pt core/shell NWs with various Pt coverages.** Concentrations are in unit of Mm [0.001 mol/Liter]. Due to the differences in volumes of 10 mM  $\text{Pt}^{4+}$  precursors and 0.1 M ascorbic acid, the total volume and the concentration of Au NWs in the final solution varied.

## S8. X-ray diffraction of Au/Pt core/shell NWs

The powder form of Au/Pt core/shell NWs were analyzed by using Cu  $K_{\alpha}$  radiation and a Rigaku RU300 powder diffractometer. The Au/Pt core/shell NWs appeared to fit very well with pure Au, but a closer look to the XRD peak pattern from the Au/Pt core/shell NWs revealed the un-symmetric shoulder peaks, in the direction of larger  $2\theta$  values. The incremental peaks are considered as an overlapping of the peaks from Au and Pt, and the XRD intensity data from the first peak of Au to that of Pt could be divided into the sharp Au peak and the broad Pt peak. The smaller particle size and thinner shell of Pt relative to that Au core resulted in much weaker diffraction from Pt despite the similar atomic weight and its location at outer shell.<sup>2</sup>

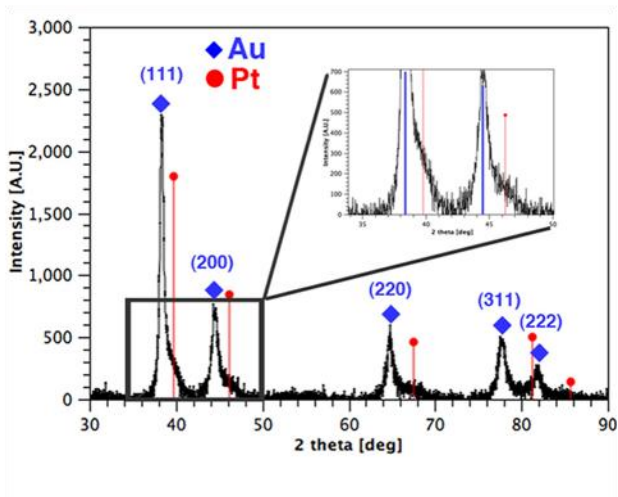


**Fig. S8. XRD result of Au/Pt core/shell NWs.** The strong XRD peaks from Au/Pt core/shell NWs from atomic ratio of (1.8:1.0) also matched with the peaks of Au crystal but the small broad peaks arising from the Pt shell were also observed. Diamonds represents the peak position of pure Au crystal and circles for Pt.

### S9. Comparison of the mapping result of Au/Pt core/shell NWs with atomic ratio of 1:1 and 2.6:1

The mapping results of the Au/Pt core/shell NWs clearly show the different surface of NWs. For the NWs with atomic ratio of 1:1 (50% Pt), the outmost surface is covered with Pt atoms as proved by UV-Vis absorption data and the CV. However, when the Pt loading amounts are reduced to 2.6:1 (28% Pt), Pt NPs on the surface of Au NW cannot completely cover the Au core.

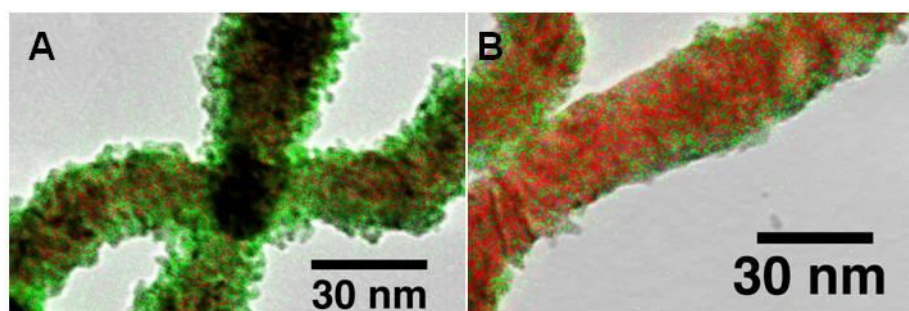


**Fig. S9.** Mapping result of Au/Pt core/shell NWs with different Pt coverages. (A)-1:1 and (B)-2.6:1. Both the Au and Pt atoms are detected on the surface of NWs of ratio of 2.6:1.

#### References for Supporting Information

1. G. Tremiliosi-Filho, L. H. Dall'Antonia and G. Jerkiewicz, *J. Electroanal. Chem.*, 1997, **422**, 149-159.
2. S. Zhou, K. McIlwrath, G. Jackson and B. Eichhorn, *J. Am. Chem. Soc.*, 2006, **128**, 1780-1781.